Carbon at Si(111)-twins: TEM analysis supported by molecular dynamics structure relaxations

Kurt Scheerschmidt[*] and **Martina Werner**

Max-Planck-Institute of Microstructure Physics, 06120 Halle, Germany

Dedicated to Professor Dr. Johannes Heydenreich on the occasion of his 75th birthday

Carbon supersaturation and high density of twin lamellae influence the physical properties of multi-crystalline silicon and restrict its applicability as a material in photovoltaics. To understand, e.g., the resulting structural modifications and the stress relief, the carbon incorporation in silicon has to be investigated by total energy minimizations using molecular dynamics simulations either at ab-initio level or applying classical methods with empirical potentials. The relaxed structure models support the interpretation of transmission electron micrographs by contrast simulations and thus the analysis of carbon incorporation at twins or elsewhere in silicon.
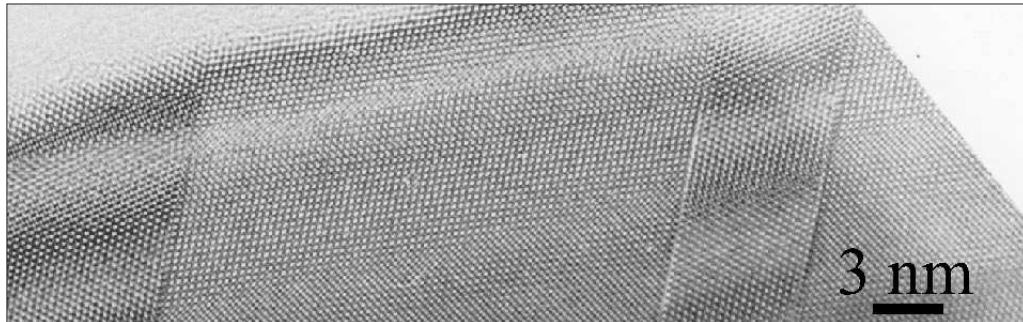
1 Introduction

Multi-crystalline silicon (mc-Si) generally contains impurities and crystal defects with a higher concentration than found in single-crystalline Si, which influence its applicability as a material in photovoltaics. The edge-defined film-fed growth (EFG) is a ribbon growth, which allows wafer production of high quality with a high output and at low cost for solar cell applications [1]. However, macroscopically, EFG wafers are characterized by high local mechanical stresses, which are up to five times higher than in other mc-Si materials [2]. Transmission electron microscope (TEM) investigations demonstrated that in these strained regions a high density (up to 10^3–10^4 cm^{-1}) of twin lamellae occurred, which, however, cannot explain the formation of local stresses in general. Besides, the non-uniform stress cannot be caused by dislocations. SiC precipitates are not found in TEM investigations. Therefore impurities, especially carbon incorporation at the twins, may be of importance to explain the phenomena. Particularly EFG wafers are highly supersaturated with carbon concentrations of up to 10^{18} cm^{-3} [3]. To investigate the problem of C-incorporation a combination of different TEM-techniques is applied [4]. Especially high resolution electron microscopy (HREM) has the ability to investigate the C-incorporation at an atomic level. However, such quantitative HREM analysis needs image contrast interpretations based on suitable atomic structure models. The present paper deals with ab-initio and empirical molecular dynamics (MD) structure relaxations [5–7] by which the accumulation of carbon at (111)-twin boundaries can be analysed using special TEM imaging conditions or alternative techniques [8, 9].

2 Experiments

Conventional diffraction contrast investigations were performed on a Phillips CM20 Twin microscope at 200 kV. HREM micrographs are made at an JOEL JEM 4010 at 400 kV, and for EDX the Phillips CM20

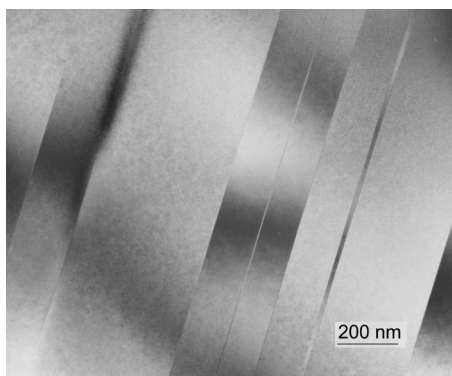[*] Corresponding author: e-mail: schee@mpi-halle.de, Phone: +49 345 5582910, Fax: +49 345 5511223

Fig. 1   HREM micrograph of a $\langle 110 \rangle$ oriented sample with {111}-twin boundaries changing their contrast due to the crossing thickness contours.
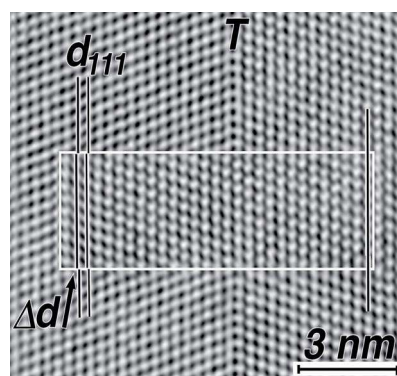
FEG capability was used. The electron optical analysis was carried out on $\langle 110 \rangle$ oriented samples with the {111}-twin boundaries parallel to the electron beam (cf. a typical HREM micrograph in Fig. 1 and the bright-field diffraction contrast image in Fig. 2). The TEM images clearly allow the analysis of the twin lamellae, however, precipitates or an increase of C at the twins cannot be observed in such a manner. EDX line scans revealed the presence of higher carbon concentration at the microtwin boundaries [4]. For C-incorporation at the twins a reduction of the lattice distance is predicted. To reveal this prediction the lattice distances in experimental micrographs are measured as demonstrated in Fig. 3, where the twin boundary is marked by T. To measure changes of the perpendicular lying {111} planes, templates of undisturbed Si lattice regions were inserted as shown by the box in the center. On the right side, the fringes of twinned lattice and the undisturbed matrix are aligned by their peaks of fringe intensities. On the left a shift of the {111} fringes of about $\Delta d = 0.4 \pm 0.1$ Å is detectable. This shift is extended over 2 to 3 planes. The MD structure simulations described in the following chapter allow to analyse these predictions in detail and to enhance the interpretation of the TEM contrast investigations.
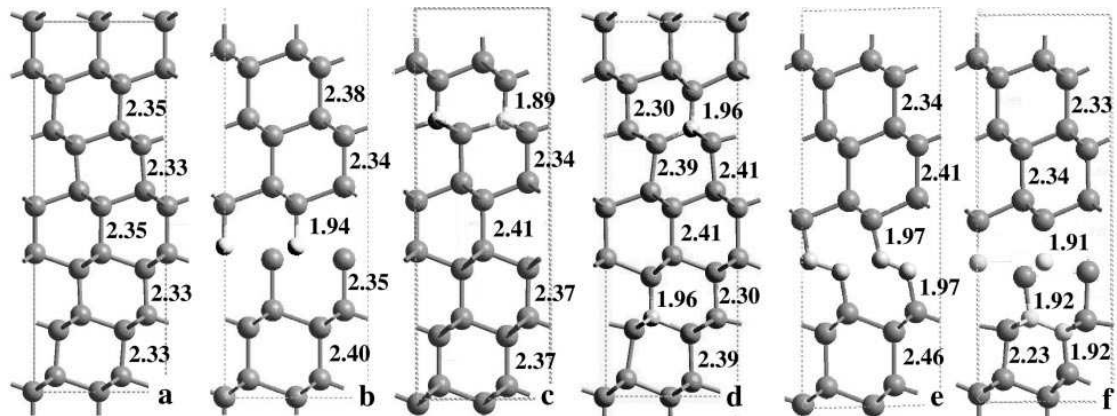
3   Structure modeling

Quantum-theoretical ab-initio simulations of different interface and defect structures as well as empirical molecular dynamics relaxations are performed to minimize the total energy of the twin boundaries (cf. [5−7]). The density functional theory (DFT) optimization of energies and atom positions (cf. examples of Fig. 4) were carried out with the code CASTEP applying ultra-soft norm-conserving pseudopotentials within the local density and/or generalized gradient approximation (LDA or GGA). The wave functions

Fig. 2   Bright-field TEM contrast of {111} twin lamellas showing bending of the microtwins.

Fig. 3   HREM micrograph of a $\langle 110 \rangle$ oriented twin boundary T. To demonstrate the reduction Δd of the {111} planes at the boundary, an image of non-disturbed Si matrix is inserted.
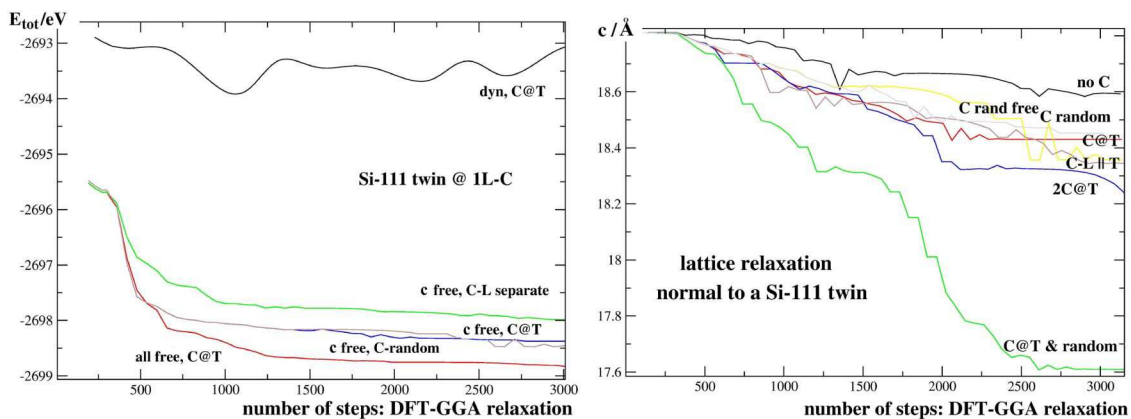
Fig. 4 Models resulting from ab-initio structure simulations (DFT approximation, cf. text) to minimize the total energy: a) Si twin structure (T) with a {111} lattice plane distance of 3.14 Å as average of the two adjacent atom layers (numbers indicate the important next neighbor distances in Å); b) half of (111) twin double plane (C@T) occupied with C (brighter spheres); c) one C-layer parallel to the twin (C-separate); d) randomly distributed C-substitutions (C-random); e) double layer of C-occupation (2C@T) at the twin yielding an additional lattice shift; f) half twin C-occupation and randomly distributed C-near the twin (C@T&random).
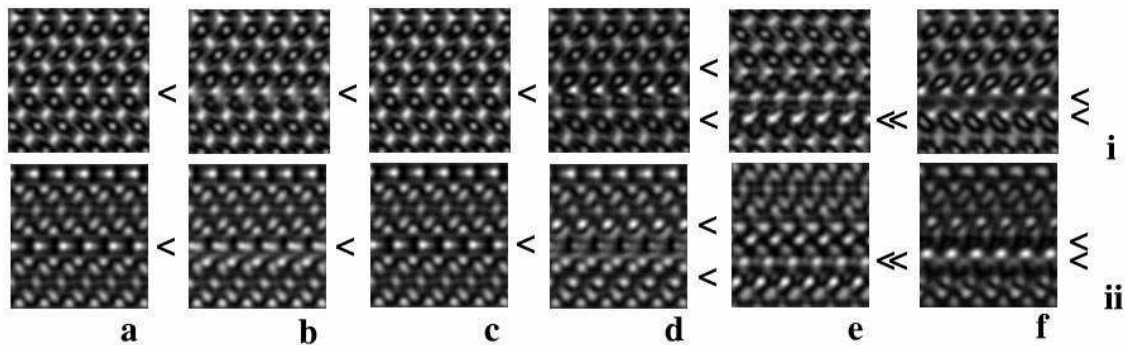
are expanded using a plane wave basis with an energy cutoff of 280 eV and symmetrized k-points according to the Monkhorst and Pack schema.

For larger systems, as, e.g., shown in Fig. 8 with 54 000 atoms and various twin layers, the only possibility of simulating time dependent atomic processes with macroscopic relevance is the molecular dynamics (MD) method solving Newton's equations of motion for all particles and using suitably fitted many-body empirical potentials, preferably of the Tersoff (TS) or bond-order type. The calculations are done using a constant pressure (NpT ensemble, relaxation at 0 K, and annealing up to 900 K) and time steps of the order of 0.8 fs (cf. [8, 9]).

Figure 4 shows the small silicon (111)-twin structure models resulting from ab-initio relaxations and describing segregation of C at the twins. Starting from a geometric twin model (24 atoms in a 6.65 Å × 18.81 Å × 3.84 Å supercell = [112]/2 × 3[111] × [110]/2 box, all bond lenghts are equal to 2.35 Å) the C atoms are substituted at one of the twin planes (b, f, C@T) or both layers (e, 2C@T) are replaced. For comparison C is also substituted additionally in layers parallel to the twin (c) or randomly in the bulk (d, f). Different processes (minimization or dynamics) and boundary conditions (various fixed vs. variable supercell borders) yield different structure reorientations, different resulting bond lengths

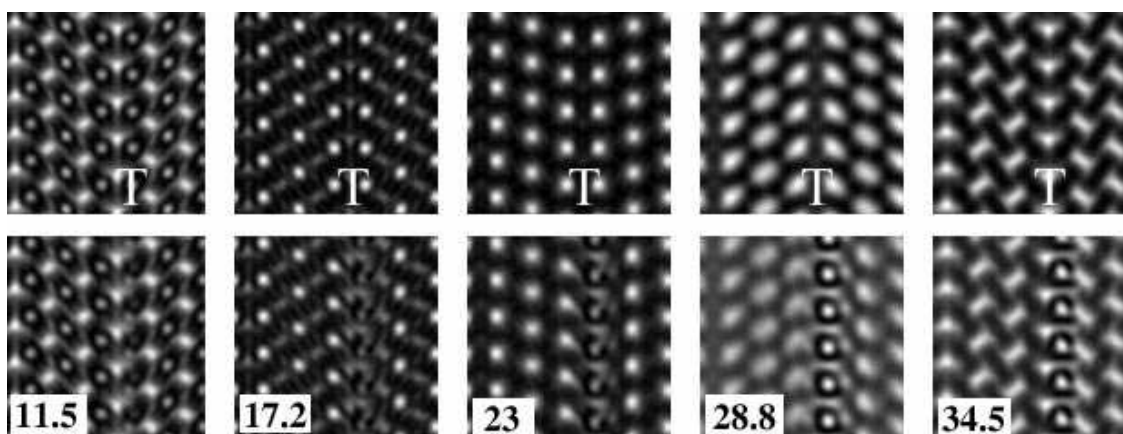**Fig. 5** (online colour at: www.pss-a.com)   Total energy (E_{tot} in eV) and extension of the supercell (c-axis in Å) normal to the twin as function of the DFT-GGA relaxation: different models and boundary conditions labeled according to Fig. 4.

phys. stat. sol. (a) **202**, No. 12 (2005) / www.pss-a.com

2371

Fig. 6 Simulated 400 kV-⟨110⟩-HREM images of the relaxed twins corresponding to the models of Fig. 4 with in different manner incorporated C atoms (thickness $t = 11.5$ nm, spherical aberration $C_s = 1$ mm, defocus spread 10 nm, beam divergence 0.5 mrad, i: Scherzer –, ii: Gauss – focus; twins or C marked by arrows).
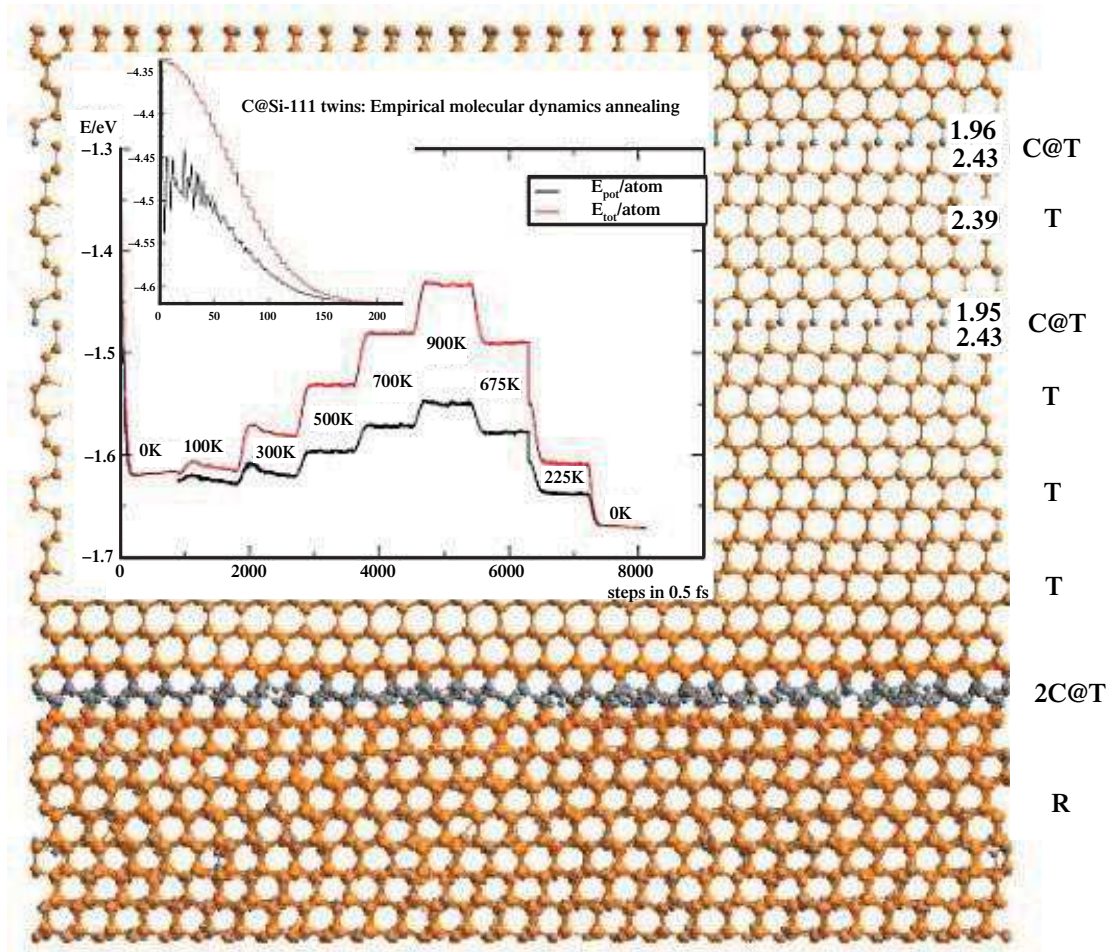
and thus lattice fringe modifications at the twins. The energy gain for the models shown in Figs. 4a) to f)is 0.34, 2.3, 1.6, 2.9, 6.1 and 5.8 eV/atom, respectively, compared always with the non-relaxed, geometric twin start model (however, d–f with all cell borders free). The curves of the total energy (cf. Fig. 5, energy difference start vs. relaxed) demonstrate that ab-initio dynamics needs much more steps for equilibration, whereas free c-axis yield 2.5 eV/atom energy gain for C@T and C random, but 3 eV/atom if all axis are free. Whereas the relaxation of the pure Si twin (Fig. 4a) results in less than 0.1% bond length rearrangements near the twin (min 2.33 Å and thus $d_{111} = 3.14$ Å lattice fringes, given as average of both adjacent atom layers), the incorporation of C (cf. Fig. 4b) yields to a drastic bond length modification of 1.94 Å at the twin and thus $d_{111} = 2.95$ Å lattice fringes. Thus in the energy minimized lattice the distance of the horizontal {111} planes is reduced by about 0.2 Å near the twin. The overall structural relaxation indicated by the modification of the c-axis during the relaxation (cf. Fig. 5) yield 0.4 Å, 0.6 Å and 1.2 Å for the cases b), e) and f) of Fig. 4, respectively.

Figure 6 shows simulated 400 kV-⟨110⟩-HREM images for a sample thickness $t = 11.5$ nm and two different defoci $\Delta f = 40$ nm (i), 0 nm (ii), corresponding to the relaxed structures (a–f) of Fig. 4. The image size is 1.9×1.9 nm^2. The lattice relaxation of the models can also be found in the image contrast, but varying with the assumed models and imaging conditions as demonstrated in Fig. 7. Here simulated 400 kV-⟨110⟩-HREM thickness series for an ideal {111}-Si twin (upper row, the twins are indicated by T) and for a C occupied twin boundary (lower row, corresponding to the model of Fig. 4b, 2C@T). The

Fig. 7 Calculated 400 kV-⟨110⟩-HREM thickness series (t in nm, $C_s = 1$ mm, $\Delta f = 40$ nm near Scherzer focus, defocus spread 10 nm, beam divergence 0.5 mrad) for a relaxed ideal {111}-Si twin (upper row) and a twin boundary containing C atoms (lower row).
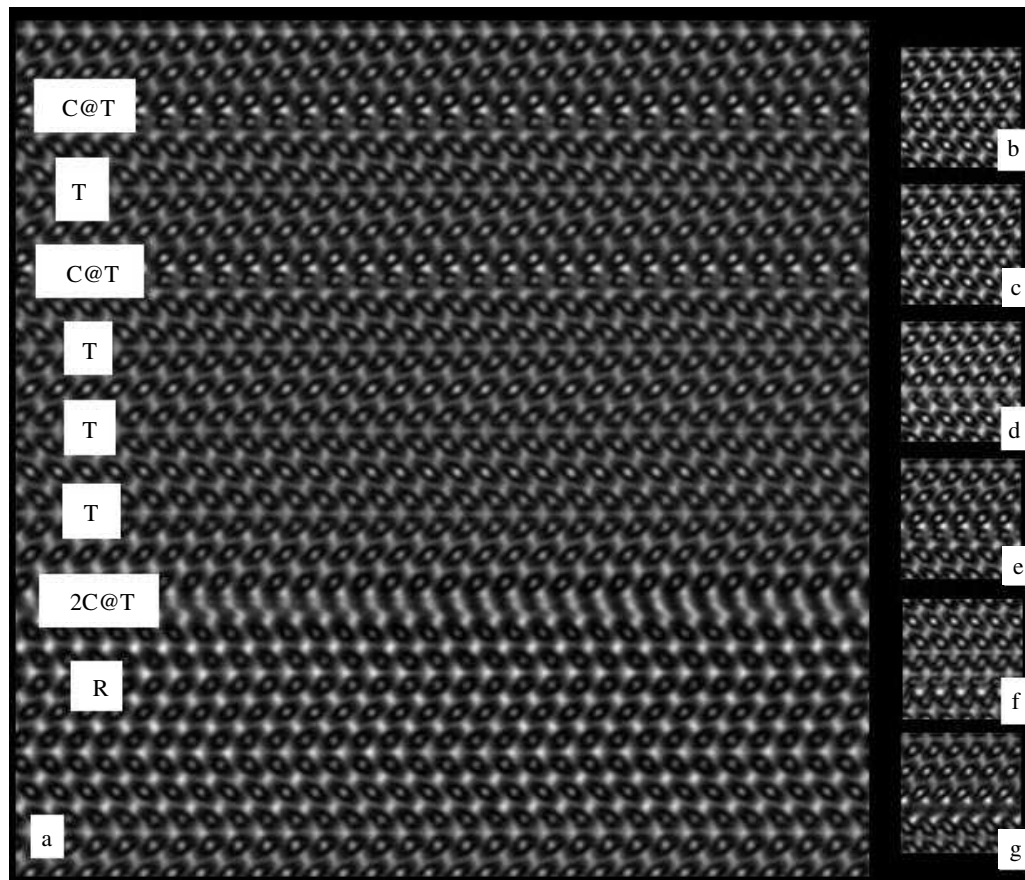
Fig. 8 (online colour at: www.pss-a.com)   MD-relaxed model (54000 atoms, TS potential) with (111)-twins (T), half (C@T) or double (2C@T) layer C-occupation, and random C-substitution (R). Inset: relative total and potential energy per atom during equilibration at the different temperature steps.

simulations demonstrate that imaging conditions exist which reveal the substitutional C in the twin boundary. The detailed analysis and a unique interpretation, however, separating alternative models and including diffusion and precipitation, needs image matching of defocus-thickness series.

Figure 8 shows a large structure model with 54000 atoms and different twin structures relaxed with empirical MD as mentioned above (9.38 nm × 9.34 nm × 11.52 nm   supercell = 7[112] × 10[111] × 15[110] box). The inset demonstrates the equilibration of the total and the potential energy during the stepwise annealing up to 900 K. The behaviour of the different twin structures and the resulting bond lengths and lattice fringe distances are very similar to those resulting from the ab-initio calculations discussed above with 3.3 eV/atom energy gain averaged over the whole structure and resulting 1.96 Å bond length at the twin and 2.43 Å for the next neighbours. However, along the double layer (2C@T) structure rearrangements and distortions are observed due to the large stresses. In addition, randomly distributed C shows clustering effects with disturbed surroundings. Both effects principally cannot be observed in energy minimizations, and because of the small supercells and short calculation times also ab-initio MD is not able to do such simulations. Using the relaxed model of Fig. 8 after cooling down to 0 K the 400 kV HREM micrographs of Fig. 9 are simulated with the same parameters as of Fig. 5. The insets (c–f) show for comparison selected twin structures from the ab-initio models for the same thickness
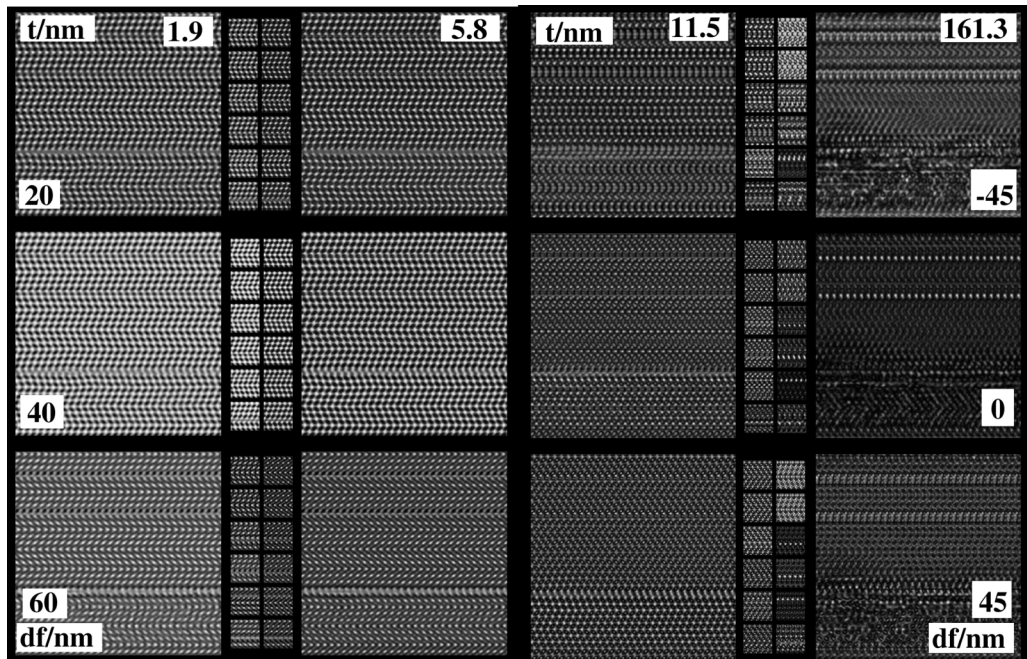
phys. stat. sol. (a) **202**, No. 12 (2005) / www.pss-a.com

2373

Fig. 9 Image simulations of Si-{111}-twin structures: (a) relaxation using empirical MD with the TS potential and 54000 atoms according to Fig. 8, (b) non-relaxed twin, (c) ab-initio relaxed twin (T), (d) non-relaxed C@T, (e) relaxed (C@T) half layer C-occupation, (f) double (2C@T) layer C-occupation, (g) random C-substitution (R) from Fig. 4.

calculated by repeating the supercell in the beam direction. Figure 9b, c, and d are the non-relaxed, relaxed twin (T), and the non-relaxed C@T, respectively, showing no contrast differences and the same contrast as in the corresponding regions of Fig. 9a. The half plane occupation at the twins (cf. Fig. 9e, which is the case C@T of Figs. 4b and 6b) shows also the same contrast as the corresponding region in Fig. 9a, i.e., a combination of small and brighter dots indicating the C-segregation at the twin. However, the strongest contrast occurs always for the double layer C-segregation at the twin (2C@T). Due to the different relaxation of the small and the larger models one yield different contrast features for the double layer C-occupation as well as additional randomly distributed carbon. The selected micrographs out of thickness-defocus series in Fig. 10 can be discussed in analogy to Fig. 9: For thin samples ($t < 6$ nm) the image simulations with the ab-initio models are always equivalent to the images of the MD relaxed structures, for thicker objects, however, the stronger relaxation yield different contrast features and additional streaks etc.

4 Discussion and conclusion

Image simulations as given in Figs. 6, 7, 9, and 10 as well as an detailed analysis of thickness-defocus series demonstrate that imaging conditions exist for which C-segregation at twins in Si clearly should be
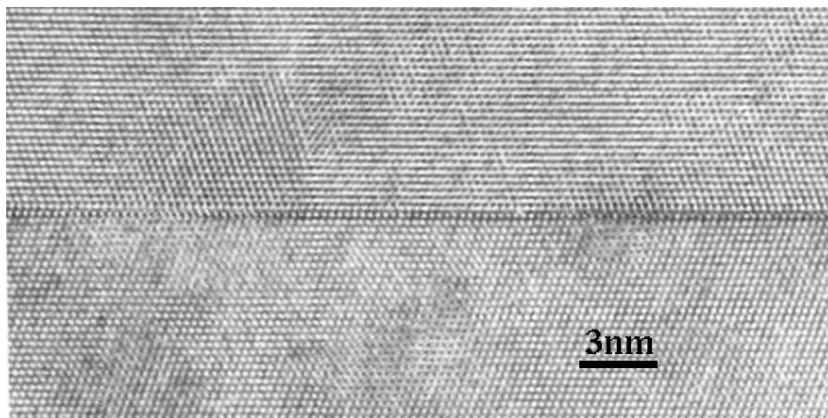
Fig. 10 Image simulations of Si-{111}-twin structures for different sample thickness (*t* in nm) and focus (d*f* in nm) comparing the MD relaxed model (large micrographs) with ab-initio relaxations (inserts, arrangement cf. Fig. 9).

revealed by TEM. The comparison of the simulations for differently modelled structures as basis of the image interpretation show the importance of the relaxation to understand the contrast details.
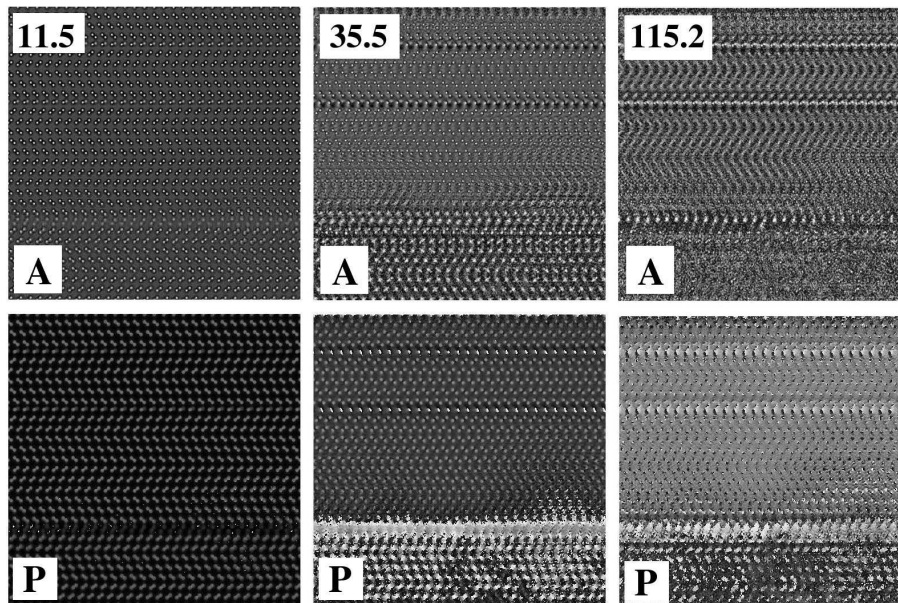
Whereas the contrast difference between relaxed and non-relaxed twins due to the small changes of bond lengths and resulting lattice fringe distances can be neglected, different C incorporation in the bulk and C segregation at the twins clearly can be discriminated using suitable imaging conditions.

In addition, the strong relaxation of carbon layers at the twin or non-homogeneity of the random distributions of carbon in the bulk may allow an explanation of the contrast variations along the experimental HREM micrograph in Fig. 11, which occur probably due to C-incorporation, remaining strains or

Fig. 11 400 kV-⟨110⟩-HREM micrograph of a Si-{111}-twin with varying contrast due to bending of the sample, carbon segregation and/or strain.

Fig. 12 Amplitudes A and Phases P for the MD relaxed model of Fig. 8 for different thicknesses *t* in nm.

bended samples. The contrast variations are here yielding from carbon rearrangements at the interfaces and resulting deformations.

However, despite the possibility to reveal different C arrangements at the twins, a quantitative analysis may be impossible in conventional TEM and HREM because of the difficulty to determine exactly the imaging conditions. Here, as Fig. 12 demonstrates, alternative techniques like defocus series reconstruction or direct imaging of amplitudes and phases using electron holography may be helpful, because in the exit wave of the object the structural details can be much better revealed. Related investigations as well as a detailed discussion of the imaging conditions will be the subject of a forthcoming paper.

References

[1] W. Schmidt, B. Woesten, and J. P. Kalejs, Prog. Photovolt., Res. Appl. **10**, 129 (2002).
[2] H. J. Möller, C. Funke, A. Lawerenz, S. Riedel, and M. Werner, Sol. Energy Mater. Sol. Cells **72**, 403 (2002).
[3] J. P. Kalejs, Solid State Phenom. **95–96**, 159 (2004).
[4] M. Werner, K. Scheerschmidt, E. Pippel, C. Funke, and H. J. Möller, IoPP Conf. Ser. **180**, 65 (2003).
[5] D. Conrad and K. Scheerschmidt, Phys. Rev. B **58**, 4538 (1998).
[6] K. Scheerschmidt, D. Conrad, A. Y. Belov, and D. Timpel, Mater. Sci. Semicond. Process. **3**, 129 (2000).
[7] K. Scheerschmidt, D. Conrad, and A. Y. Belov, Comput. Mater. Sci. **24**, 33 (2002).
[8] K. Scheerschmidt and M. Werner, in: Proc. 13th European Microscopy Congress, edited by D. Schryvers and J.-P. Timmermans, Vol. 1 (Belgian Society for Microscopy, Liège, Belgium, 2004), pp. 105–106.
[9] M. Werner and K. Scheerschmidt, in: Proc. 13th European Microscopy Congress, edited by D. Schryvers and J.-P. Timmermans, Vol. 2 (Belgian Society for Microscopy, Liège, Belgium, 2004), pp. 403–404.